Appl. Math. Mech. -Engl. Ed., **45**(4), 677–694 (2024)

APPLIED MATHEMATICS AND MECHANICS (ENGLISH EDITION)

https://doi.org/10.1007/s10483-024-3089-5

Study of hybrid nanofluid flow in a stationary cone-disk system with temperature-dependent fluid properties*

A. S. JOHN[1], B. MAHANTHESH[1,2], G. LORENZINI[3,†]

1. Center for Mathematical Needs, Department of Mathematics, CHRIST (Deemed to be University), Karnataka 560029, India;
2. School of Mathematical and Statistical Sciences, The University of Texas Rio Grande Valley, Texas 78539, U. S. A.;
3. Department of Engineering and Architecture, University of Parma, Parma 43124, Italy

(Received Jun. 5, 2023 / Revised Dec. 11, 2023)

Abstract Cone-disk systems find frequent use such as conical diffusers, medical devices, various rheometric, and viscosimetry applications. In this study, we investigate the three-dimensional flow of a water-based Ag-MgO hybrid nanofluid in a static cone-disk system while considering temperature-dependent fluid properties. How the variable fluid properties affect the dynamics and heat transfer features is studied by Reynolds's linearized model for variable viscosity and Chiam's model for variable thermal conductivity. The single-phase nanofluid model is utilized to describe convective heat transfer in hybrid nanofluids, incorporating the experimental data. This model is developed as a coupled system of convective-diffusion equations, encompassing the conservation of momentum and the conservation of thermal energy, in conjunction with an incompressibility condition. A self-similar model is developed by the Lie-group scaling transformations, and the subsequent self-similar equations are then solved numerically. The influence of variable fluid parameters on both swirling and non-swirling flow cases is analyzed. Additionally, the Nusselt number for the disk surface is calculated. It is found that an increase in the temperature-dependent viscosity parameter enhances heat transfer characteristics in the static cone-disk system, while the thermal conductivity parameter has the opposite effect.

Key words hybrid nanofluid, cone-disk system, laminar flow, variable fluid property, Nusselt number

Chinese Library Classification O267, O357
2010 Mathematics Subject Classification 76D05, 76R05, 80A20, 82D80

1 Introduction

The past few decades have indicated an exponential increase in energy demand which has

* Citation: JOHN, A. S., MAHANTHESH, B., and LORENZINI, G. Study of hybrid nanofluid flow in a stationary cone-disk system with temperature-dependent fluid properties. *Applied Mathematics and Mechanics* (*English Edition*), **45**(4), 677–694 (2024) https://doi.org/10.1007/s10483-024-3089-5
† Corresponding author, E-mail: giulio.lorenzini@unipr.it

led to energy shortage and environmental pollution. This has caused an urgent need to conserve existing energy. Statistics predict an increase of 48% over the next 2 decades alone due to the expanding population. A plausible solution to overcome this limitation could improve heat transfer and reduce effective heat dissipation in various applications. This can be done by using nanofluids as the operating fluid in industries. Nanofluids are colloidal suspensions containing nanometer-sized particles. The addition of such ultra-fine particles in regular fluids was seen to augment the heat transfer properties of regular fluids like water, oils, and ethylene glycol. Choi[1] developed the revolutionary method of improving heat transmission, by suspending nano-sized particles in the base fluids. This helped eradicate the barriers experienced by conventional fluids in obtaining maximum thermal performance, by suspending uniformly tiny-sized particles with a nanoparticle volume fraction of less than 5%. This category of fluids then became a potential area for research due to its improved stability, and enhanced thermal, electrical, and mechanical properties[2]. Another advantage of nanofluids is the flexibility to alter their composition for various applications, which led to a wide range of applications capable of reforming the entire field of heat transfer. Those included protein detection, drug, and gene delivery in biomedical science to absorption of solar and geothermal energy, automotive cooling, heat exchangers, chillers, radiators, and nuclear coolants in industries.

In general, the thermal behavior of nanofluids is studied using two well-known theoretical models, namely, the Khanafer-Vafai-Lightstone (KVL) mono-phasic nanofluid model[3] and the Buongiorno bi-phase model[4]. The former model assumes no slippage and the existence of a local thermal equilibrium between the two fluid phases. This implies that the nanofluid behaves more like a classical Newtonian liquid, with both the base fluid and nanoparticles having the same local velocity and temperature, in contrast to the solid-liquid mixture considered in the conventional bi-phase model. The effective properties of the base fluid were explained by phenomenological relations and the mixture theory. Experimental data showed that better heat transfer occurs when the nanoparticle concentration is dilute. Tiwari and Das[5] utilized a single-phase mathematical model for nanofluids that incorporates the volume percentage of nanoparticles.

The requirement for a cooling agent with more efficiency in heat transfer led to the novel discovery of hybrid nanofluid which is a homogenous suspension of more than one nanoparticle amalgamated in a base fluid. Because of the synergistic effects, hybridizing the appropriate nanoparticles can aid in altering the pressure drop and heat transfer rates. The increased heat transfer rate and advanced thermal properties made its usage suitable in microchip cooling, solar collectors, heat sinks, pipes, and exchangers. The ideal combination of diverse nanoparticles ensures improvement in both the thermal and rheological properties of the resultant nanofluid. Oxides like Al_2O_3, MgO, etc. are known for their stability and chemical inertness but are restricted by low thermal conductivity. On the other hand, particles like Ag, Cu, and Al have much better thermal conductivity but poor stability and chemical inertness. Hence, the combination of such nanoparticles helps tradeoff between the pros and cons of using a single nanoparticle. Much more research has been conducted on hybrid nanofluids to critically comprehend the preparation procedures, properties, stability, and many applications[6–8]. The superiority in rheological and thermophysical properties in comparison with other fluids makes it a prominent topic of research.

Temperature gradients highly impact the physical properties of the fluid. Machine lubrication, production of glass fiber or paper, extraction of crude oil, metal extrusion, hot rolling, geothermal systems, and several other physical processes have differences in the temperature gradients. Incorporating the temperature-dependent fluid properties helps capture the complete dynamics of the heat transport features. Herwig et al.[9] provided factual evidence that fluid properties like thermal conductivity and viscosity are very susceptible to temperature variations, which tend to alter the nature of the fluid flow. They analyzed the case of water and noticed that the viscosity drastically decreased with an increase in temperature. This was ac-

counted for by the growth in the transport phenomena consequently causing heat transfer at the walls. The practical applicability of such inclusion has led many researchers to investigate flows involving variable viscosity over multiple geometry configurations[10–12]. Meanwhile, Chiam[13] evaluated the influence of variable thermal conductivity on heat transfer over a stretching sheet, by considering thermal conductivity as a linear function of temperature. As a result, to evaluate the heat transmission of the flow accurately, utilization of the variable fluid characteristics is of utmost importance. The problem at hand, therefore, attempts to include such variations in the thermophysical fluid properties, by considering the fluid viscosity and thermal conductivity as a function of temperature.

The geometrical configuration of the cone and disk apparatus is of much significance due to its wide spectrum of applications in several fields including biomedical research. This apparatus finds itself useful in analyzing Oldroyd-B creeping flow's stability[14], in stationary conical diffusers to compress air[15], and in viscosimetry[16]. Rheometers, which are instruments used to calculate viscosity, and normal friction coefficients have also adopted a similar geometry. Such devices are crucial for determining and managing the viscosities of liquids like ink, varnishes, glues, etc. Additionally, its use can also be observed in the sealing of rotating shafts, in bio-medical devices that culture endothelial cells, in measuring oxygen concentration, as well as in the convective diffusion of the feeding cultures[17]. Being a prospective area of research, many researchers have studied various aspects of fluid flow using this cone-disk framework. Fewell and Hellums[18] obtained the numerical solution for the flow amidst the cone and disk apparatus when a very small conical gap is taken. This was further validated experimentally by Sdougos et al.[19]. Shevchuk[20] conducted research in this area and highlighted characteristic features of fluid flow and heat transfer in the cone-disk system. He obtained the Navier-Stokes (NS) momentum equation for a cone-disk system in the self-similar form. Simulations were done in Ref. [21], to analyze the steady-state axisymmetric flow of air in the cone-disk system. This was carried out by keeping the disk at a radially dependent temperature and the cone at a constant temperature. The velocity and thermal profiles were interpreted for cases when either the disk or the cone was stationary, or when both were in rotation. A complementary study was done to scrutinize the influence of Prandtl (Pr) and Schmidt (Sc) numbers in the rotating cone-disk system[22]. This was done by varying the parameters Pr and Sc over a range of 0.1 to 800 when the disk was in rotation, and over a range of 0.1 to 100 when the cone was in rotation. Potential applications and scope of fluid flow in a cone-disk system were also included in his study. Recently, Shevchuk[23] has obtained analytical solutions for the simplified NS equations in a cone-disk system with conicity less than 5° for a non-swirling flow, using the asymptotic series expansion method. Gul et al.[24] examined the temperature and concentration distribution in the conical gap of the cone disk equipment incorporating magnetic effects. Turkyilmazoglu[25–26] indicated the necessity of considering the radial diffusive terms to estimate the rate of heat transfer precisely. The extreme use of the cone disk configuration inspired numerous researchers like Srilatha et al.[27], Moatimid et al.[28], Wang et al.[29], Basavarajappa and Bhatta[30–31] to consider different physical aspects to analyze the heat transport in a cone-disk apparatus.

Interestingly, many of the studies concerning the cone-disk system assume either one, or both components in rotation. However, studies concerning the stationary cone-disk system, with fluid flow caused by an external swirling device are very limited. Comprehensive literature indicates that the modeling of fluid flow in a stationary cone-disk system was first reported by Shevchuk[32]. He derived self-similar variables to transform the equations modeling the fluid flow in a stationary conical diffuser and, provided physical interpretation of the boundary conditions used. Heat transport features and the Nusselt number calculations, of the laminar swirled flow of a clean fluid (air) in a stationary cone-disk system, were presented for the first time in these works. Further, a detailed description and the modeling of the flow caused by an external swirler at the inlet of a stationary conical diffuser were provided in Ref. [21]. The influence of

pre-swirl, as well as several non-dimensional parameters on the thermal and velocity profiles was examined. However, in these studies, the fluid properties were considered to be constant. To the best of the authors' knowledge, studies concerning nanofluids in static cone-disk systems with temperature-dependent properties are open questions.

Therefore, the scope of the present work is to examine the Ag-MgO-H_2O hybrid nanofluid flow in the conical gap between a stationary cone and a disk subject to variable fluid properties. The chief objectives of the present analysis are as follows.

(I) Develop a mathematical model for the Ag-MgO-H_2O hybrid nanofluid flow in a stationary cone-disk system.

(II) Determine how the temperature-dependent viscosity and thermal conductivity affect the flow pattern and heat transfer features of Ag-MgO-H_2O composite nanofluid in the cone-disk system.

(III) Obtain a self-similar equation model using the one-parameter Lie-group theory.

(IV) Perform comparisons between swirling and non-swirling flows.

(V) Analyze the Nusselt number at the disk surface.

The remaining part of the paper is structured as follows. The mathematical formulation and physical configuration are presented in Section 2. It also consists of the governing equations specific to the problem along with appropriate boundary conditions. The similarity transformations employed to obtain the self-similar equations are explained in Section 3. Section 4 highlights the validity and other pertinent details of the numerical procedure. This is followed by the results in Section 5 which are discussed with the help of tables and graphs. Finally, Section 6 provides a summary of the key findings.

2 Mathematical formulation

A steady and laminar flow of hybrid nanofluids is considered, in a stationary conical disk system. The cylindrical coordinate system (r, φ, z) is taken, where r represents the radial axis, φ represents the azimuthal axis, and z represents the axial axis (see Fig. 1). The two-component framework comprises a non-rotating disk positioned at $z = 0$ and a cone positioned at $z = h$, the gap of which is occupied by the Ag-MgO-H_2O hybrid nanofluid. The conical gap height is $r\tan\gamma$, where γ is the angle between the cone and disk surface. The fluid flow is caused by a flow swirler device[21,32]. Isothermal temperatures are maintained at the walls of the disk T_d and cone T_c, the difference of which causes effective heating up of the fluid. The bisector of the gap angle at $z = \frac{h}{2}$ is neither a cone nor a solid surface. The study considers the thermal transfer that occurs in the lower portion, i.e., between the bisector interface and the disk surface. The bisector interface is assumed to have a constant temperature T_b. The mathematical models for fluid flow in a static cone-disk system are presented in the monographs[21,33].

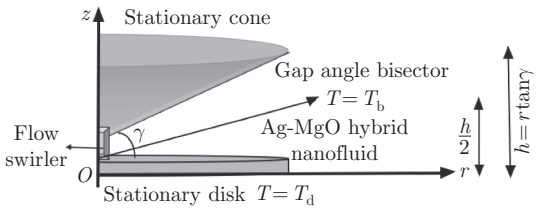

Fig. 1 Physical configuration of the stationary conical diffuser problem (color online)

Furthermore, the following assumptions are taken to analyze the problem.

(I) The Ag and MgO particles which are of sizes 25 nm and 40 nm orderly, are dispersed in water in equal proportions. The KVL model is adopted, which utilizes phenomenological and effective medium laws to describe the effective nanofluid characteristics[3]. The state of local

thermal equilibrium is maintained throughout by the nanometer-sized particles as well as the base fluid. The fluid and the nanoparticles have the same relative velocity throughout. The base fluid properties such as viscosity and thermal conductivity are temperature-dependent.

(II) The Boussinesq approximation is employed.

(III) The slow flow and incompressible fluid make the impact of viscous dissipation negligible.

(IV) By following Shevchuk[34], the radial diffusion terms in the energy equation are not disregarded, as the conicity angle considered in the study is 35°.

The governing equations of mass, linear momentum, and energy specified for an incompressible hybrid nanofluid are as follows.

The conservation of mass is

$$\nabla \cdot \boldsymbol{U} = 0, \tag{1}$$

the conservation of momentum is

$$\rho_{\mathrm{hnf}}\Big(\frac{\partial \boldsymbol{U}}{\partial t} + \boldsymbol{U}\cdot\nabla\boldsymbol{U}\Big) = -\nabla p + \nabla\cdot(\mu_{\mathrm{hnf}}(T)\nabla\boldsymbol{U}), \tag{2}$$

and the conservation of energy is

$$(\rho c_p)_{\mathrm{hnf}}\Big(\frac{\partial T}{\partial t} + \boldsymbol{U}\cdot\nabla T\Big) = \nabla\cdot(\kappa_{\mathrm{hnf}}(T)\nabla T), \tag{3}$$

where $\boldsymbol{U} = (u, v, w)$ is the velocity matrix along the directions (r, φ, z), respectively, t is the time, $\rho, \mu, (\rho c_p)$, and κ represent the density, viscosity, heat capacitance, and thermal conductivity of the hybrid nanofluid, respectively, p is the pressure, T is the temperature of the nanofluid, $\nabla(\cdot) = \frac{\partial(\cdot)}{\partial r} + \frac{1}{r}\frac{\partial(\cdot)}{\partial \varphi} + \frac{\partial(\cdot)}{\partial z}$ is the gradient operator, and the subscript 'hnf' stands for hybrid nanofluid.

For a steady-state axisymmetric flow, the following are the component forms of governing equations (see Refs. [21], [32], [35], [36], and [37]):

$$\Big(\frac{\partial u}{\partial r} + \frac{u}{r} + \frac{\partial w}{\partial z}\Big) = 0, \tag{4}$$

$$\rho_{\mathrm{hnf}}\Big(u\frac{\partial u}{\partial r} - \frac{v^2}{r} + w\frac{\partial u}{\partial z}\Big) = -\frac{\partial p}{\partial r} + \frac{\partial}{\partial r}\Big(\mu_{\mathrm{hnf}}(T)\frac{\partial u}{\partial r}\Big) + \frac{\partial}{\partial r}\Big(\mu_{\mathrm{hnf}}(T)\frac{u}{r}\Big) + \frac{\partial}{\partial z}\Big(\mu_{\mathrm{hnf}}(T)\frac{\partial u}{\partial z}\Big), \tag{5}$$

$$\rho_{\mathrm{hnf}}\Big(u\frac{\partial u}{\partial r} - \frac{uv}{r} + w\frac{\partial v}{\partial z}\Big) = \frac{\partial}{\partial r}\Big(\mu_{\mathrm{hnf}}(T)\frac{\partial v}{\partial r}\Big) + \frac{\partial}{\partial r}\Big(\mu_{\mathrm{hnf}}(T)\frac{v}{r}\Big) + \frac{\partial}{\partial z}\Big(\mu_{\mathrm{hnf}}(T)\frac{\partial v}{\partial z}\Big), \tag{6}$$

$$\rho_{\mathrm{hnf}}\Big(u\frac{\partial w}{\partial r} + w\frac{\partial w}{\partial z}\Big) = -\frac{\partial p}{\partial z} + \frac{\partial}{\partial r}\Big(\mu_{\mathrm{hnf}}(T)\frac{\partial w}{\partial r}\Big) + \frac{1}{r}\frac{\partial}{\partial r}(\mu_{\mathrm{hnf}}(T)w) + \frac{\partial}{\partial z}\Big(\mu_{\mathrm{hnf}}(T)\frac{\partial w}{\partial z}\Big), \tag{7}$$

$$(\rho c_p)_{\mathrm{hnf}}\Big(u\frac{\partial T}{\partial r} + w\frac{\partial T}{\partial z}\Big) = \frac{\partial}{\partial r}\Big(\kappa_{\mathrm{hnf}}(T)\frac{\partial T}{\partial r}\Big) + \frac{\kappa_{\mathrm{hnf}}(T)}{r}\frac{\partial T}{\partial r} + \frac{\partial}{\partial z}\Big(\kappa_{\mathrm{hnf}}(T)\frac{\partial T}{\partial z}\Big). \tag{8}$$

To solve Eqs. (4)–(8), the following boundary conditions are used (see Refs. [21] and [32]):

$$\begin{cases} \text{at} \quad z = 0\colon \quad u = 0, \quad v = 0, \quad w = 0, \quad T = T_{\mathrm{d}}, \\ \text{at} \quad z = z_1\colon \quad u = u_1, \quad v = v_1, \quad \dfrac{\partial u}{\partial z} = 0, \quad T = T_{\mathrm{b}}, \end{cases} \tag{9}$$

where $z_1 = \frac{r}{2}\tan\gamma$, and the subscript '1' denotes the boundary conditions at the center of the gap angle where the free vortex develops, representing an exemplar free vortex pattern. The fluid at the inlet to the gap close to the coordinate $r = 0$ has non-zero tangential and radial velocity components. This causes the fluid to move radially outwards, having the swirl components $u = u_1 = \frac{F_1\mu_0}{r}$ and $v = v_1 = \frac{G_1\mu_0}{r}$, specified in accordance with the free vortex

law[21,32]. Furthermore, the bisector is kept at a constant temperature, distinct from that of the cone, except when $r = 0$, meaning that, the fluid at the bisector interface is not affected by the heat transfer since it develops radially outwards along increasing radii. As the gap widens and the local radius expands, any temperature variation across the gap does not affect the fluid at the bisector.

The effective density and specific heat capacity are modeled by the mixture theory[38–39],

$$\frac{\rho_{\mathrm{hnf}}}{\rho_{\mathrm{f}}} = (1-\phi_{\mathrm{MgO}})\Big(1-\phi_{\mathrm{Ag}}\Big(1-\frac{\rho_{\mathrm{Ag}}}{\rho_{\mathrm{f}}}\Big)\Big)+\phi_{\mathrm{MgO}}\frac{\rho_{\mathrm{MgO}}}{\rho_{\mathrm{f}}} = \mathscr{B}, \tag{10}$$

$$\frac{(\rho c_p)_{\mathrm{hnf}}}{(\rho c_p)_{\mathrm{f}}} = (1-\phi_{\mathrm{MgO}})\Big(1-\phi_{\mathrm{Ag}}\Big(1-\frac{(\rho c_p)_{\mathrm{Ag}}}{(\rho c_p)_{\mathrm{f}}}\Big)\Big)+\phi_{\mathrm{MgO}}\frac{(\rho c_p)_{\mathrm{MgO}}}{(\rho c_p)_{\mathrm{f}}} = \mathscr{C}, \tag{11}$$

where ϕ_{Ag} represents the nanoparticle volume fraction (NVF) of the Ag nanoparticle, ϕ_{MgO} represents the NVF of the magnesium oxide nanoparticle, and the subscript 'f' represents the base fluid (water).

Esfe et al.[40] proposed an experimental model to determine the thermophysical properties of the Ag-MgO nanofluid, based on regression analysis and curve fitting of experimental data. The dynamic viscosity and thermal conductivity of Ag-MgO are taken in correspondence to this model as

$$\frac{\mu_{\mathrm{hnf}}(T)}{\mu_{\mathrm{f}}(T)} = 1+32.795\phi-7\,214\phi^2+714\,600\phi^3-0.194\,1\times10^8\phi^4 = \mathscr{A}, \tag{12}$$

$$\frac{\kappa_{\mathrm{hnf}}(T)}{\kappa_{\mathrm{f}}(T)} = \frac{\phi+1.747\times10^4}{1.997\,7\times10^7\phi^3+1.117\times10^6\phi^2-1.498\times10^5\phi+1.747\times10^4} = \mathscr{D}, \tag{13}$$

where $\phi = \phi_{\mathrm{Ag}} + \phi_{\mathrm{MgO}}$ is the total NVF of the Ag-MgO-H_2O hybrid nanofluid, considered to be between 0–2%, as these values have good correspondence with the experimental model.

The symbols $\mathscr{A}, \mathscr{B}, \mathscr{C}$, and $\mathscr{D}$ are used to denote the expressions $\frac{\mu_{\mathrm{hnf}}}{\mu_{\mathrm{f}}}$, $\frac{\rho_{\mathrm{hnf}}}{\rho_{\mathrm{f}}}$, $\frac{(\rho c_p)_{\mathrm{hnf}}}{(\rho c_p)_{\mathrm{f}}}$, and $\frac{\kappa_{\mathrm{hnf}}}{\kappa_{\mathrm{f}}}$, respectively. In Eqs. (12) and (13), μ_{f} and κ_{f} are temperature-dependent.

The base fluid properties like viscosity (μ_{f}) and thermal conductivity (κ_{f}) are defined as functions that vary with temperature linearly. The linearized Reynolds's viscosity model is considered for viscosity[41],

$$\mu_{\mathrm{f}}(T) = \mu_0\Big(1-\alpha\frac{T-T_{\mathrm{b}}}{\Delta T}\Big), \tag{14}$$

where α indicates the parameter of variable viscosity, μ_0 is the uniform reference dynamic viscosity, and $\Delta T = T_{\mathrm{d}} - T_{\mathrm{b}} > 0$.

As in Chiam's proposed model[13], the variable thermal conductivity is taken as

$$\kappa_{\mathrm{f}}(T) = \kappa_0\Big(1+\beta\frac{T-T_{\mathrm{b}}}{\Delta T}\Big), \tag{15}$$

where β indicates the thermal conductivity parameter, and κ_0 is the uniform reference thermal conductivity.

3 Self-similar method

Lie-group analysis is used to develop invariant self-similar transformations, which aid in the conversion of the modeled partial differential equations (PDEs) to the corresponding ordinary differential equations (ODEs). This systematic and efficient technique has been utilized by multiple researchers to study the fluid flow characteristics resulting from various flow configurations. The following self-similar variables are obtained. Details on the derivation of these

transformations can be seen in Refs. [21], [30], [31], and [37],

$$\eta = \frac{z}{r}, \quad F(\eta) = \frac{ur}{\mu_0}, \quad G(\eta) = \frac{vr}{\mu_0}, \quad H(\eta) = \frac{wr}{\mu_0}, \quad P(\eta) = \frac{pr^2}{\rho_{\mathrm{f}}\mu_0^2}, \quad \theta(\eta) = \frac{T - T_{\mathrm{b}}}{\Delta T}, \tag{16}$$

where η is the similarity variable, and $F(\eta)$, $G(\eta)$, and $H(\eta)$ are the non-dimensional velocities along the r, φ, and z axes dependent on the self-similar variable η, respectively. $P(\eta)$ and $\theta(\eta)$ represent the non-dimensional pressure and temperature, respectively.

Equations (14) and (15) are expressed in dimensionless forms as follows:

$$\mu_{\mathrm{f}}(\theta) = \mu_0(1 - \alpha\theta), \tag{17}$$

$$\kappa_{\mathrm{f}}(\theta) = \kappa_0(1 + \beta\theta). \tag{18}$$

Using Eqs. (16)–(18) and Eqs. (10)–(13), the set of Eqs. (4)–(8) subject to the conditions (9) takes the subsequent form of ODEs as

$$H' - \eta F' = 0, \tag{19}$$

$$\mathscr{A}\chi\Lambda F'' + (\mathscr{A}(3\chi\eta - \Lambda\alpha\theta') - \mathscr{B}(H - \eta F))F' + \mathscr{B}(F^2 + G^2) + 2P + \eta P' = 0, \tag{20}$$

$$\mathscr{A}\chi\Lambda G'' + (\mathscr{A}(3\chi\eta - \Lambda\alpha\theta') - \mathscr{B}(H - \eta F))G' = 0, \tag{21}$$

$$\mathscr{A}\chi\Lambda H'' + (\mathscr{A}(3\chi\eta - \Lambda\alpha\theta') - \mathscr{B}(H - \eta F))H' + (\mathscr{A}\chi + \mathscr{B}F)H - P' = 0, \tag{22}$$

$$(1 + \beta\theta)\Lambda\theta'' + (\mathscr{D}(1 + \beta\theta)\eta - \mathscr{C}Pr(H - \eta F))\theta' + \mathscr{D}\Lambda\beta\theta'^2 = 0, \tag{23}$$

where $\Lambda = 1 + \eta^2, \chi = 1 - \alpha\theta$, the prime $'$ denotes the derivative with respect to η, and Pr represents the Prandtl number, which is a non-dimensional parameter. It quantifies the impact caused by momentum diffusivity and thermal diffusivity and is defined as $Pr = \frac{\mu_0(c_p)_{\mathrm{f}}}{\kappa_0}$. The Pr value of the base fluid water is calculated to be 6.067 4, using the thermophysical properties of water at 300 K.

The transformed boundary conditions are as follows:

$$\begin{cases} \text{at} \quad \eta = 0: \quad F = 0, \quad G = 0, \quad H = 0, \quad \theta = 1, \\ \text{at} \quad \eta = \eta_1: \quad F = F_1, \quad G = G_1, \quad F' = 0, \quad \theta = 0, \end{cases} \tag{24}$$

where $\eta_1 = \frac{1}{2}\tan\gamma$, and F_1 and G_1 are constants, for the case when a free vortex is created by the radial and azimuthal velocities at $\eta = \eta_1$. Alternatively, the boundary conditions imply that swirling flow develops as a free vortex along the gap angle bisector[32].

One can also eliminate the pressure from Eqs. (20) and (22) to get

$$\begin{aligned} &\mathscr{A}\chi\Lambda^2 F''' + \Lambda(\eta(10\mathscr{A}\chi + \mathscr{B}F) - \mathscr{B}H - 2\mathscr{A}\alpha\Lambda\theta')F'' \\ &+ (3(\mathscr{A}\chi(2 + 7\eta^2) + \mathscr{B}(1 + 2\eta^2)F - \mathscr{B}\eta H) - \mathscr{A}\alpha\Lambda(10\eta\theta' + \Lambda\theta''))F' \\ &+ 2\mathscr{B}GG' + (3(\mathscr{A}\chi + \mathscr{B}F) - \mathscr{A}\alpha\eta\theta')H = 0. \end{aligned} \tag{25}$$

Using Fourier's heat law, the Nusselt number at the disk surface is defined as[21,30]

$$Nu_{\mathrm{d}} = \frac{r q_{\mathrm{h}}|_{z=0}}{\kappa_0 \Delta T}, \tag{26}$$

where q_{h} is the heat flux and is given by

$$q_{\mathrm{h}} = -\kappa_{\mathrm{hnf}} \frac{\partial T}{\partial z}. \tag{27}$$

The dimensionless Nusselt number (Nu_{d}) at the disk surface becomes

$$Nu_{\mathrm{d}} = -\mathscr{D}(1 + \beta)\theta'(0). \tag{28}$$

4 Solution methodology

The non-linear system of differential equations (19)–(23) poses complexity making it extremely difficult to solve it analytically. Thus, these equations are solved numerically using the MATLAB solver (finite difference method-based solver). This function helps find solutions to boundary value problems (BVPs) containing differential equations of degree one,

$$y'(x) = f(x, y(x), \Im), \quad x \in [L, R]$$

along with the two-point boundary conditions of $0 = \mathscr{G}(x_L, x_R, y(x_L), y(x_R), \Im)$. Here, $\mathscr{G}$ denotes the initial conditions, and $\Im$ symbolizes the vector whose parameters are to be determined[42]. The run time and efficiency of the solver depend on the initial guess value. Further details concerning the methodology are available in our earlier publications[30–31].

The following variables are adopted to convert the higher-order ODEs to single-order ODEs:

$$(\hbar_1, \hbar_2, \hbar_3, \hbar_4, \hbar_5, \hbar_6, \hbar_7, \hbar_8) = (F, F', F'', H, G, G', \theta, \theta'). \tag{29}$$

Equation (29) yields the following first-order ODE system:

$$\hbar_1' = \hbar_2, \tag{30}$$

$$\hbar_2' = \hbar_3, \tag{31}$$

$$\begin{aligned}\hbar_3' = \frac{1}{\mathscr{A}\chi\Lambda^2}\big(&\Lambda(\eta(10\mathscr{A}\chi + \mathscr{B}\hbar_1) - \mathscr{B}\hbar_4 - 2\mathscr{A}\alpha\Lambda\hbar_8)\hbar_3 \\ &+ (3(\mathscr{A}\chi(2 + 7\eta^2) + \mathscr{B}(1 + 2\eta^2)\hbar_1 - \mathscr{B}\eta\hbar_4) - A\alpha\Lambda(10\eta\hbar_8 + \Lambda\mho))\hbar_2 \\ &+ 2\mathscr{B}\hbar_5\hbar_6 + (3(A\chi + \mathscr{B}\hbar_1) - A\alpha\eta\hbar_8)\hbar_4\big),\end{aligned} \tag{32}$$

$$\hbar_4' = \eta\hbar_2, \tag{33}$$

$$\hbar_5' = \hbar_6, \tag{34}$$

$$\hbar_6' = -\frac{1}{\mathscr{A}\chi\Lambda}(\mathscr{A}(3\chi\eta - \Lambda\alpha\hbar_8) - \mathscr{B}(\hbar_4 - \eta\hbar_1))\hbar_6, \tag{35}$$

$$\hbar_7' = \hbar_8, \tag{36}$$

$$\hbar_8' = -\frac{1}{(1 + \beta\hbar_7)\Lambda}((\mathscr{D}(1 + \beta\hbar_7)\eta - \mathscr{C}Pr(\hbar_4 - \eta\hbar_1))\hbar_8 + \mathscr{D}\Lambda\beta\hbar_2^2) = \mho, \tag{37}$$

and the boundary conditions are

$$\begin{cases} \text{at} \quad \eta = 0\colon \quad \hbar_1 = 0, \quad \hbar_5 = 0, \quad \hbar_4 = 0, \quad \hbar_7 = 1, \\ \text{at} \quad \eta = \eta_1\colon \quad \hbar_1 = F_1, \quad \hbar_5 = G_1, \quad \hbar_2 = 0, \quad \hbar_7 = 0. \end{cases} \tag{38}$$

The accuracy of the obtained results has been evaluated by comparing the Nusselt number values obtained by considering a clean fluid, specifically, air, and the Prandtl number 0.71 with those reported by Shevchuk[21] (see Table 1). This comparison highlights the consistency between the solutions, and consequently the reliability of the method is used.

5 Results and discussion

This section aims to analyze the velocity, thermal, and Nusselt number profiles of a stationary cone-disk system. The analysis is done for two different types of flow, non-swirling flow where there exists no swirl in the flow ($G_1 = 0$), and swirling flow where swirl exists in the flow ($G_1 = 97.96$). Calculations are done numerically for the fluid flow in a stationary cone-disk apparatus, with a conicity angle of 35° and $\eta_1 = 0.350\,1$[32]. Further, the effects of variable

Table 1 The rates of heat transport (Nu_{d}) of air from the surface of a disk with those provided by Shevchuk[21] when $Pr = 0.71$

F_1	$G_1 = 0$		$G_1 = 97.96$	
	Shevchuk[21]	Present result	Shevchuk[21]	Present result
2	2.891	2.890 8	2.228	2.228 1
10	3.016	3.015 7	2.311	2.310 7
20	3.147	3.147 1	2.398	2.398 0
45	3.330	3.330 4	2.532	2.531 6
63	3.320	3.320 0	2.553	2.552 6
70	3.286	3.286 1	2.545	2.545 5
90	3.123	3.122 9	2.487	2.487 4

These numerical values of Ref. [21] are provided by Prof. I. V. SHEVCHUK upon our request

fluid viscosity (α), variable thermal conductivity (β), and F_1 and G_1 on the heat transfer in the system are scrutinized using tables (see Tables 2–3) and graphs (see Figs. 2–11). In the graphs, the solid lines correspond to the Ag-MgO-H_2O nanofluid flow, and the dashed lines represent that of water.

Table 2 depicts the rate of heat transfer on the surface of a stationary disk for different values of F_1, G_1, and α. The heat transport rate (Nu_{d}) at the disk surface increases by increasing the F_1 values from 2 to 45 for non-swirling flow when $\alpha \neq 0$. However, Nu_{d} decreases for increasing F_1 values as $F_1 = 63, 70$, and 90. Introducing a swirl in the flow broadens the range over which the heat transfer increases at the disk surface. In a swirling flow with variable viscosity, the rate of heat transfer increases in the range [2, 63] after which it deteriorates. However, in the absence of variable viscosity, the increment takes place over a range of [2, 63] for a non-swirling flow and over a range of [2, 70] for a swirling flow. In addition, in a non-swirling flow, it can be noted that the increase enhances the effective heat transport at the walls of the disk till F_1 approaches 63. This trend reverses as F_1 is further increased. However, strengthening the variable viscosity parameter α in a swirling flow causes the heat transfer to decrease at the disk surface, irrespective of the F_1 value.

Table 2 The heat transport rate on the disk surface (Nu_{d}) for several values of F_1 and α when $Pr = 6.067\,4$, and $\beta = 0.3$

F_1	$G_1 = 0$				$G_1 = 97.96$			
	$\alpha = 0$	$\alpha = 0.25$	$\alpha = 0.45$	$\alpha = 0.75$	$\alpha = 0$	$\alpha = 0.25$	$\alpha = 0.45$	$\alpha = 0.75$
2	4.157 6	4.170 3	4.185 1	4.225 7	0.711 7	0.446 7	0.270 6	0.136 0
10	5.162 5	5.226 5	5.299 6	5.499 1	1.053 5	0.665 2	0.389 1	0.171 3
20	6.122 6	6.234 7	6.361 7	6.703 1	1.545 7	0.996 8	0.564 8	0.212 0
45	7.287 5	7.412 0	7.547 0	7.885 4	2.623 5	1.803 3	0.979 6	0.265 4
63	7.342 2	7.376 1	7.393 5	7.322 3	2.945 8	2.029 1	1.051 1	0.251 5
70	7.221 9	7.195 5	7.133 1	6.761 3	2.959 1	2.011 2	1.011 0	0.237 7
90	6.508 1	6.229 8	5.818 8	3.691 4	2.723 1	1.709 3	0.770 0	0.187 9

Table 3 illustrates the rate of heat transfer on the surface of a stationary disk, for several values of F_1, G_1, and β. For a non-swirling flow, strengthening the F_1 parameter causes the rate of heat transfer to increase in the domain [2, 45], after which it begins to decrease. For a swirling flow, enhancing F_1 values causes the heat transfer to increase over the domain for small values of the variable thermal conductivity parameter β in the domain [2, 45]. However, greater variations in the thermal conductivity parameter cause the heat transfer to increase over the domain [2, 63] after which it deteriorates. Further, as β increases, the rate of heat transfer grows exponentially at the disk irrespective of the swirling parameter. Table 3 also indicates

that introducing a swirl in a flow with variable thermal conductivity diminishes the transfer of thermal energy at the disk surface. The impact of the thermal conductivity parameter, for both swirling and non-swirling flow, appears to be direct for the rate of heat transport at the disk surface, for all values of F_1.

Table 3 The heat transport rate on the disk surface (Nu_d) for several values of F_1 and β when $Pr = 6.067\,4$, and $\alpha = 0.6$

F_1	$G_1 = 0$				$G_1 = 97.96$			
	$\beta = 0$	$\beta = 0.5$	$\beta = 2$	$\beta = 7$	$\beta = 0$	$\beta = 0.5$	$\beta = 2$	$\beta = 7$
2	3.689 7	4.540 0	7.066 3	15.479 9	0.052 0	0.315 8	2.044 8	9.894 6
10	4.813 8	5.741 9	8.314 7	16.626 5	0.078 4	0.408 1	2.298 3	10.318 5
20	5.840 3	6.912 6	9.690 5	17.922 4	0.117 3	0.527 1	2.588 4	10.773 3
45	6.900 8	8.179 9	11.480 3	19.968 6	0.196 9	0.740 4	3.050 5	11.450 7
63	6.626 0	7.867 7	11.022 7	19.249 3	0.192 5	0.736 8	3.066 9	11.499 9
70	6.297 7	7.485 5	10.526 1	18.653 8	0.177 4	0.701 3	3.007 0	11.432 2
90	4.643 9	5.601 3	8.252 8	16.399 9	0.120 5	0.549 6	2.705 7	11.046 6

The development of radial velocities, for non-swirling and swirling flows in the presence of variable viscosity can be analyzed from Fig. 2. In a non-swirling flow ($G_1 = 0$), the radial flow starts separating from the surface boundaries at $F_1 \sim 63$. At values below that, the flow seems to be merged with the walls, and for values above 63, there appears a significant region over the disk where recirculation occurs. The cause for this behavior is attributed to the increased conicity of the diffuser. These facts contribute to the reasoning behind the nature of the radial velocity profiles indicated in Figs. 2(a)–2(c). For small values of F_1, the radial velocity component of the non-swirling flow increases with the increase in variable viscosity. Here, the case of constant viscosity exhibits a minimum radial velocity. In addition, as the values of F_1 increase, the trend reverses, and the constant viscosity case achieves a greater radial velocity.

When the swirling parameter is increased to 97.96, there emerges an amplified recirculation

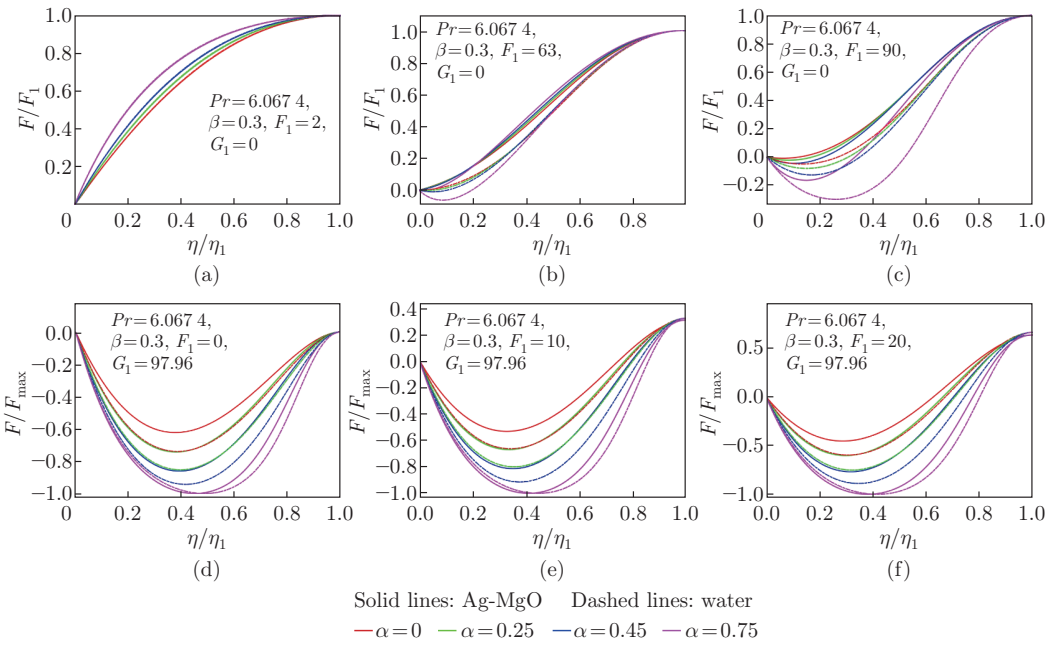

Fig. 2 Radial velocity fields for distinct values of viscosity parameter (α) when (a) $F_1 = 2$, (b) $F_1 = 63$, (c) $F_1 = 90$, (d) $F_1 = 0$, (e) $F_1 = 10$, and (f) $F_1 = 20$ (color online)

zone over the surface of the disk. Strengthening the F_1 value causes enhancement in the recirculation zone. Further, the flow caused by centrifugal forces decays as it approaches the middle of the disk-bisector interface. This accounts for the shape of the graphs in Figs. 2(d)–2(f). The trends in these velocity profiles for both swirling and non-swirling flows are in line with those reported by Shevchuk[21,32]. Further, a swirling flow with constant viscosity achieves a maximum radial velocity, in contrast to that of a non-swirling flow.

The development of the radial velocities for the nanofluid flow with variable thermal conductivity (see Figs. 3(a)–3(f)) is analogous to that of variable viscosity (see Figs. 2(a)–2(f)). Further, they also coincide with the results presented by Shevchuk[21,32]. For small values of the F_1 parameter, the variation of thermal conductivity does not create changes in the radial velocities of a non-swirling flow. The growth of the thermal conductivity decreases the radial velocity in case of a non-swirling flow. Meanwhile, in a swirling flow, the radial velocity is enhanced by the thermal conductivity. A similar trend was also observed in the work by Animasaun[43], wherein he studied the effect of temperature-dependent variable viscosity and thermal conductivity on the heat transfer of a nanofluid flow along a vertical plate.

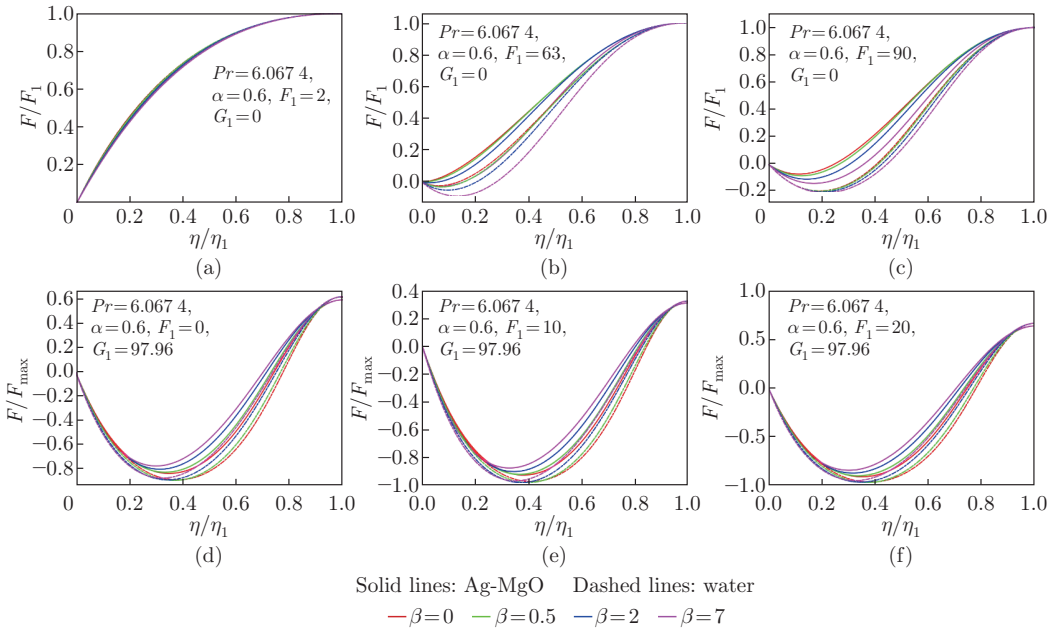

Fig. 3 Radial velocity fields for distinct values of thermal conductivity parameter (β) when (a) $F_1 = 2$, (b) $F_1 = 63$, (c) $F_1 = 90$, (d) $F_1 = 0$, (e) $F_1 = 10$, and (f) $F_1 = 20$ (color online)

The development of the tangential velocities for the swirling flow can be seen in Figs. 4 and 5. From Fig. 4, it can be observed that the maximum tangential velocity is attained when the variable viscosity parameter is 0.25, followed by $\alpha = 0$, $\alpha = 0.45$, and $\alpha = 0.75$, irrespective of the F_1 value. As the variable viscosity parameter increases, the tangential profiles lose their linear nature gradually. Figure 5 indicates that increasing the thermal conductivity parameter increases the tangential velocities for all values of F_1. It is evident that the tangential velocity profile varies linearly between the disk ($\eta = 0$) and the bisector ($\eta/\eta_1 = 1$). This result agrees with that provided by Shevchuk[21,33]. Further, higher tangential velocities appear for the hybrid nanofluid in comparison to pure water.

Figures 6 and 7 show that in a non-swirling flow, there is an exponential increase in the axial velocities, with the lowest being at the boundaries of the disk and the highest at that of the bisector interface. In the case where variable viscosity is incorporated, a unique behavior is

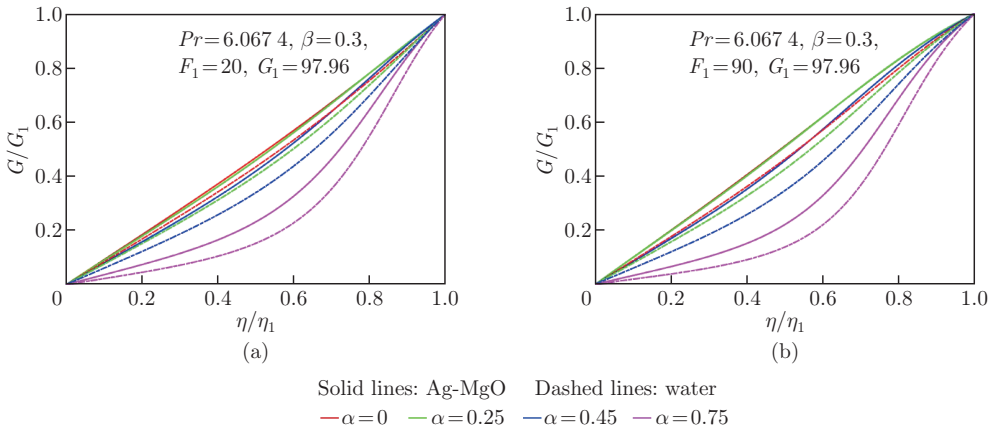

Fig. 4 Tangential velocity fields (G/G_1) for distinct values of viscosity parameter (α) when (a) $F_1 = 20$ and (b) $F_1 = 90$ (color online)

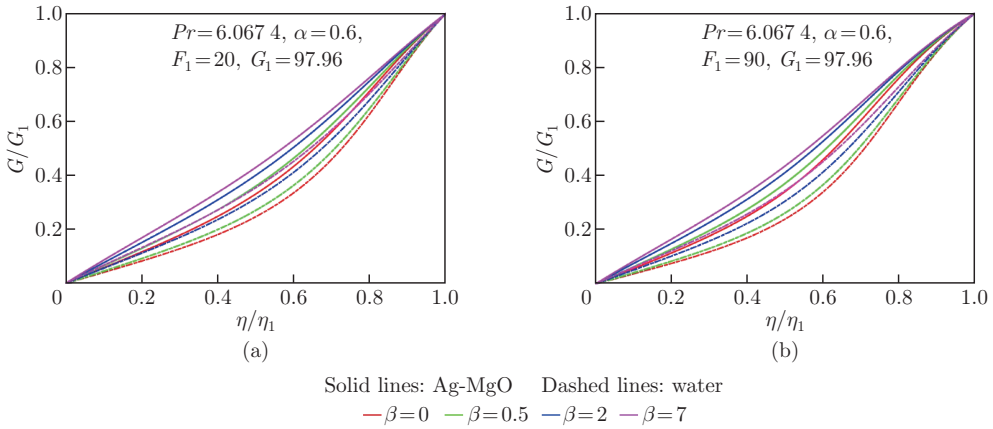

Fig. 5 Tangential velocity fields (G/G_1) for distinct values of thermal conductivity parameter (β) when (a) $F_1 = 20$ and (b) $F_1 = 90$ (color online)

recognized. For lower values of F_1, enhancing variable viscosity α reduces the axial velocities at the bisector interface, and increases the same at the disk. Meanwhile, for larger values of F_1 approximately larger than 55, we can observe an opposite trend, where there is a direct relation of variable viscosity parameter and radial velocity at the bisector and an inverse relation of the same at the disk surface. Further, the variable thermal conductivity parameter β is directly proportional to the component of axial velocity at the bisector and inversely proportional to the same at the disk.

In the case of swirling flow as seen in Figs. 8 and 9, the axial velocity profile obtained by varying viscosity as well as thermal conductivity is analogous. It deteriorates gradually until it reaches a minimum, which happens at approximately $\eta/\eta_1 = 0.5$, followed by a rapid increase. Consequently, the axial velocity at the bisector is higher than that of the disk. An increase in the variable viscosity diminishes the axial velocity at the disk and enhances the same at the bisector. In all the above figures (see Figs. 2–9) representing the velocity profiles, we can scrutinize the impact of nanoparticles. The presence of ultra-refined nanometer-sized particles can be seen to enhance the radial velocity as well as the tangential velocity. These outcomes align with the findings reported in Refs. [44] and [45]. Furthermore, greater velocity components are observed at the bisector interface in comparison with that of the disk.

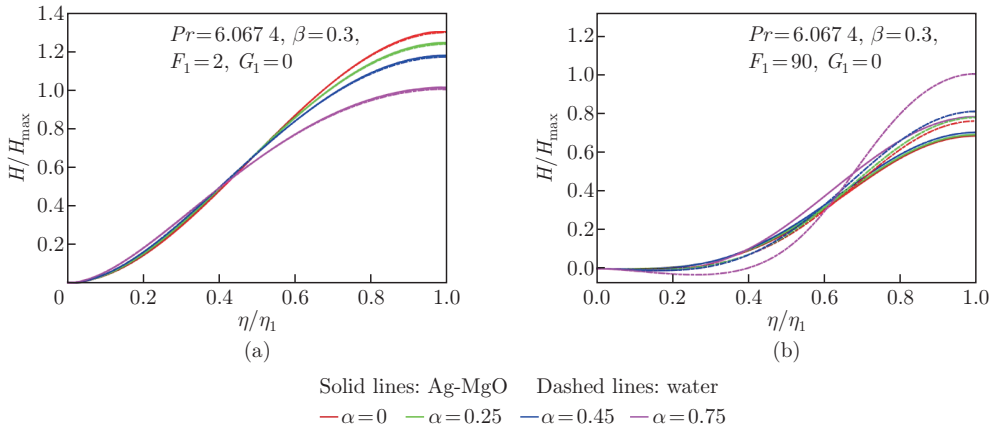

Fig. 6 Axial velocity fields ($H/H_{\max}$) of non-swirling flow for distinct values of viscosity parameter (α) when (a) $F_1 = 2$ and (b) $F_1 = 90$ (color online)

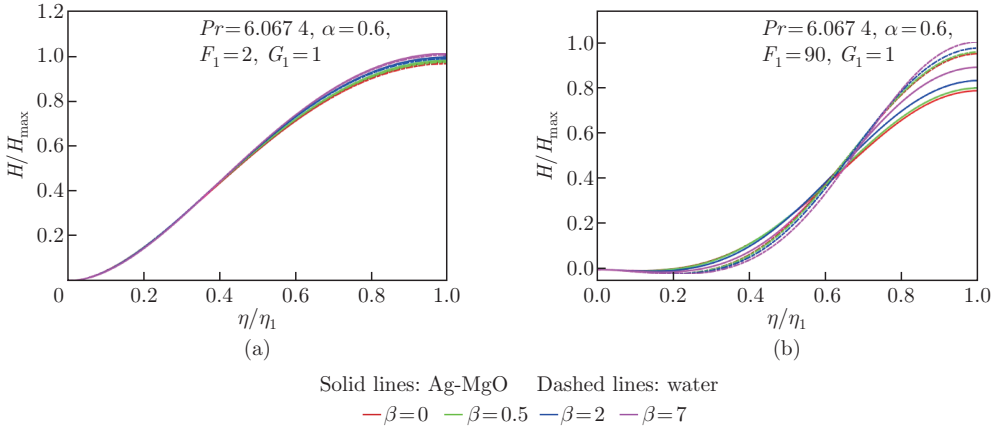

Fig. 7 Axial velocity fields ($H/H_{\max}$) of non-swirling flow distinct values of thermal conductivity parameter (β) when (a) $F_1 = 2$ and (b) $F_1 = 90$ (color online)

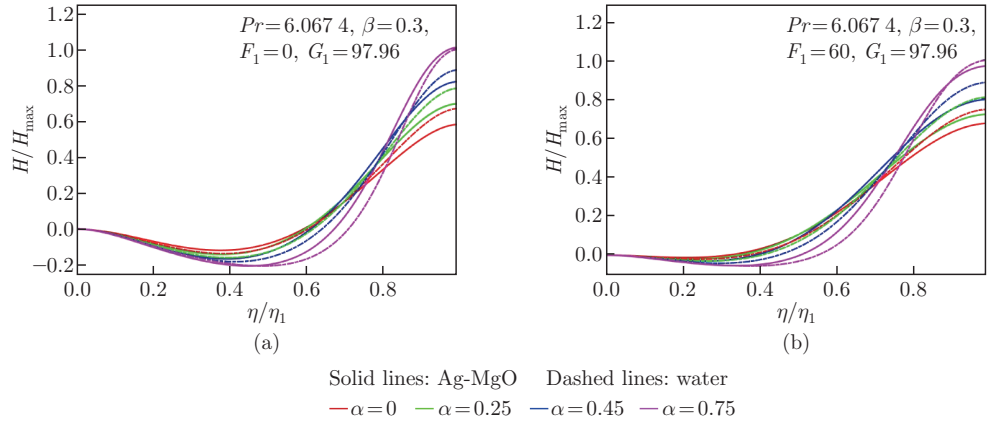

Fig. 8 Axial velocity fields ($H/H_{\max}$) of swirling flow for distinct values of viscosity parameter (α) when (a) $F_1 = 0$ and (b) $F_1 = 60$ (color online)

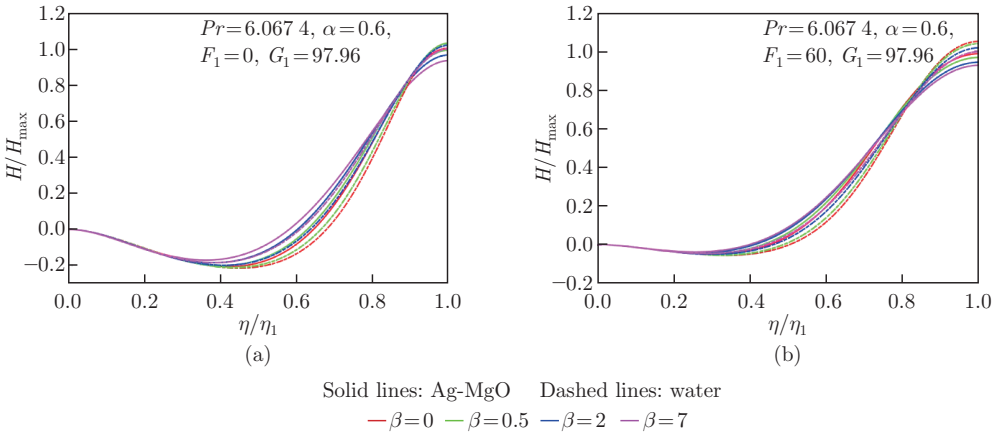

Fig. 9 Axial velocity fields ($H/H_{\max}$) of swirling flow for distinct values of thermal conductivity parameter (β) when (a) $F_1 = 0$ and (b) $F_1 = 60$ (color online)

The temperature profiles of swirling flow with variable viscosity and variable thermal conductivity, for several values of F_1 are shown in Figs. 10 and 11 respectively. The graphs in Fig. 10 indicate the direct proportionality between the viscosity parameter and the temperature. These results are similar to those obtained in Refs. [46] and [47]. As the value of F_1 increases, the temperature difference between the constant viscosity case and the variable viscosity case widens. From Fig. 9, we can infer that the growth in the thermal conductivity parameter causes the temperature to reduce. In both instances, the temperature is maximum at the disk which exponentially decays and reaches 0 at the bisector interface. Also, in all the above temperature profiles the presence of nanoparticles reduces the temperature of the apparatus.

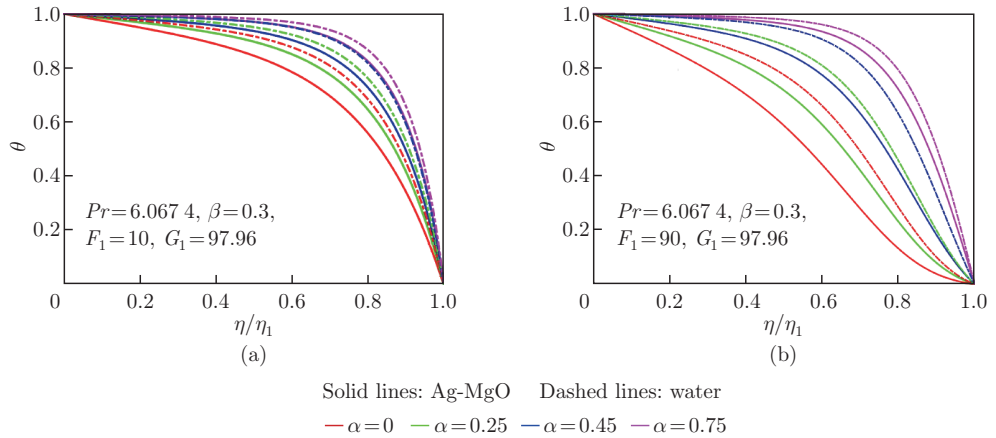

Fig. 10 Thermal fields (θ) for distinct values of viscosity parameter (α) when (a) $F_1 = 10$ and (b) $F_1 = 90$ (color online)

6 Concluding remarks

The study investigates the three-dimensional flow of the Ag-MgO-H_2O hybrid nanofluid in a stationary cone-disk system. The effects of temperature-dependent viscosity and temperature-dependent thermal conductivity are examined. The current problem can be categorized into two problems, namely, one is the swirling parameter G_1 being 0, for a non-swirling flow, and

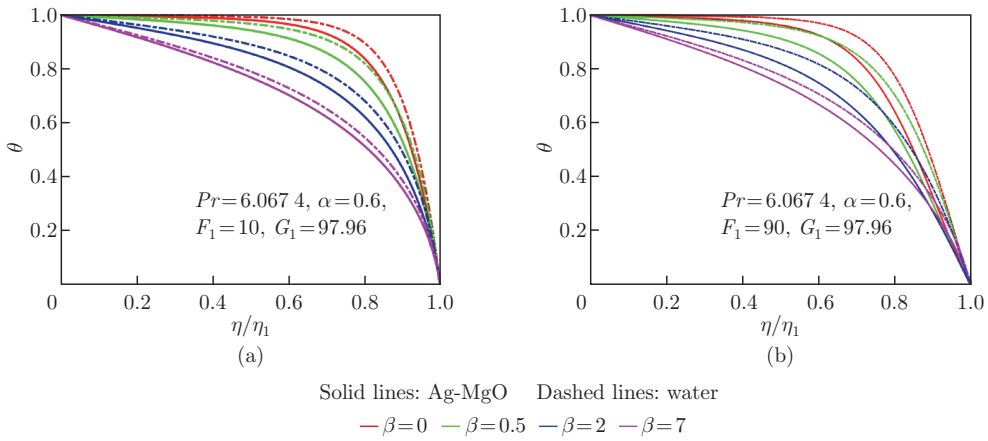

Fig. 11 Thermal fields (θ) for distinct values of thermal conductivity parameter (β) when (a) $F_1 = 10$ and (b) $F_1 = 90$ (color online)

the other is G_1 being 97.96 for a swirling flow corresponding to a conicity of 35°. The PDEs administering the flow in the cone and plate instrument are simplified into the corresponding non-dimensional ODEs using similarity variables that are specifically suitable for this problem. The results obtained by Shevchuk[21,32] can be recovered by nullifying the variable viscosity and fluid thermal conductivity parameter as well as neglecting the presence of nanoparticles and radial diffusive terms which directly guarantee the accuracy and precision of the algorithm used. The key conclusions of the study at hand can be put in a nutshell as follows.

(I) The addition of nanometer-sized particles enhances the transfer of heat which consequently causes enhancement of the transport of heat within the system. This result is also concurrent to the findings in Refs. [44] and [45].

(II) In a non-swirling flow, the radial flow is unified with the walls as the value of F_1 increases to 63, after which it starts dissociating at $F_1 = 63$ beyond which enhanced recirculation occurs. Similar results were also found in the works by Shevchuk[21,32].

(III) The azimuthal velocity component increases linearly from the surface of the disk to the bisector, and the changes caused by F_1 are almost imperceptible[21,32].

(IV) The axial velocity component at the bisector interface appears to follow a trend opposite to that of the disk surface in all cases.

(V) The heat transfer at the disk surface reaches a maximum with the variation in thermal conductivity as well as an absence of swirl in the flow.

(VI) With a swirl in the flow and increases in variable fluid properties, especially for smaller values of F_1, the heat transmission is maximized at the bisector interface.

(VII) The consequences to the temperature profiles obtained by varying viscosity and thermal conductivity are qualitatively similar. Increasing the F_1 values reduces the effective temperature of the system.

(VIII) Varying the viscosity escalates the system's temperature while varying the thermal conductivity decreases the temperature of the system.

The above problem demonstrates its uses in bio-medical devices, clinical engineering, and industrial settings, where disk-cone equipment is of much significance.

Conflict of interest The authors declare no conflict of interest.

Acknowledgements The authors are indebted to the anonymous referees for their constructive comments, which have substantially contributed to clarifying and strengthening this paper. The authors also greatly appreciate the help and discussion of Prof. I. V. SHEVCHUK, TH Köln-University of Applied Sciences, Germany.

References

[1] CHOI, S. U. S. Enhancing thermal conductivity of fluids with nanoparticles. *International Mechanical Engineering Congress and Exposition*, **66**, 613–630 (1995)

[2] NIIHARA, K. New design concept of structural ceramics ceramic nanocomposites. *Journal of the Ceramic Society of Japan*, **99**(1154), 974–982 (1991)

[3] KHANAFER, K., VAFAI, K., and LIGHTSTONE, M. Buoyancy-driven heat transfer enhancement in a two-dimensional enclosure utilizing nanofluids. *International Journal of Heat and Mass Transfer*, **46**(19), 3639–3653 (2003)

[4] BUONGIORNO, J. Convective transport in nanofluids. *ASME Heat Transfer*, **128**(3), 240–250 (2006)

[5] TIWARI, R. K. and DAS, M. K. Heat transfer augmentation in a two-sided lid-driven differentially heated square cavity utilizing nanofluids. *International Journal of Heat and Mass Transfer*, **50**(9-10), 2002–2018 (2007)

[6] SUNDAR, L. S., SHARMA, K. V., SINGH, M. K., and SOUSA, A. C. M. A review on hybrid nanofluids: recent research, development and applications. *Renewable and Sustainable Energy Reviews*, **43**, 164–177 (2015)

[7] SARKAR, J., GHOSH, P., and ADIL, A. Hybrid nanofluids preparation, thermal properties, heat transfer, and friction factor — a review. *Renewable and Sustainable Energy Reviews*, **68**, 185–198 (2017)

[8] SIDIK, N. A. C., JAMIL, M. M., JAPAR, W. M. A. A., and ADAMU, I. M. A review on preparation methods, stability and applications of hybrid nanofluids. *Renewable and Sustainable Energy Reviews*, **80**, 1112–1122 (2017)

[9] HERWIG, H., WICKERN, G., and GERSTEN, K. Influence of variable fluid properties to free convection laminar flows. *Waerme-Stoffuebertrag*, **19**(1), 19–30 (1985)

[10] POP, I., GORLA, R. S. R., and RASHIDI, M. The effect of variable viscosity on flow and heat transfer to a continuous moving flat plate. *International Journal of Engineering Science*, **30**, 1–6 (1992)

[11] SEDDEEK, M. A. Finite-element method for the effects of chemical reaction, variable viscosity, thermophoresis, and heat generation/absorption on a boundary-layer hydromagnetic flow with heat and mass transfer over a heat surface. *Acta Mechanica*, **177**(1), 1–18 (2005)

[12] MUKHOPADHYAY, S., LAYEK, G. C., and SAMAD, S. A. Study of MHD boundary layer flow over a heated stretching sheet with variable viscosity. *International Journal of Heat and Mass Transfer*, **48**(21-22), 4460–4466 (2005)

[13] CHIAM, T. Heat transfer in a fluid with variable thermal conductivity over a linearly stretching sheet. *Acta Mechanica*, **129**(1), 63–72 (1998)

[14] PHAN-THIEN, N. Cone and plate flow of the Oldroyd-B fluid is unstable. *Journal of Non-Newtonian Fluid Mechanics*, **17**(1), 37–44 (1985)

[15] OWEN, J. M. and ROGERS, R. H. Flow and heat transfer in rotating-disk systems, volume I — rotor-stator systems. *NASA STI/Recon Technical Report A*, **90**, 45759 (1989)

[16] MOONEY, M. and EWART, R. H. The conicylindrical viscometer. *Physics*, **5**(11), 350–354 (1934)

[17] SPRUELL, C. and BAKER, A. B. Analysis of a high-throughput cone-and-plate apparatus for the application of defined spatiotemporal flow to cultured cells. *Biotechnology and Bioengineering*, **110**(6), 1782–1793 (2013)

[18] FEWELL, M. E. and HELLUMS, J. D. The secondary flow of Newtonian fluids in cone-and-plate viscometers. *Transactions of the Society of Rheology*, **21**(4), 535–565 (1977)

[19] SDOUGOS, H. P., BUSSOLARI, S. R., and DEWEY, C. F. Secondary flow and turbulence in a cone-and-plate device. *Journal of Fluid Mechanics*, **138**, 379–404 (1984)

[20] SHEVCHUK, I. V. A self-similar solution of Navier-Stokes and energy equations for rotating flows between a cone and a disk. *High Temperature*, **42**(1), 104–110 (2004)

[21] SHEVCHUK, I. V. *Convective Heat and Mass Transfer in Rotating Disk Systems*, Springer, New York (2009)

[22] SHEVCHUK, I. V. Laminar heat and mass transfer in rotating cone-and-plate devices. *Journal of Heat Transfer*, **133**(2), 024502 (2011)

[23] SHEVCHUK, I. V. An asymptotic expansion method vs a self-similar solution for convective heat transfer in rotating cone-disk systems. *Physics of Fluids*, **34**(10), 103610 (2022)

[24] GUL, T., BILAL, M., ALGHAMDI, W., ASJAD, M., and ABDELJAWAD, T. Hybrid nanofluid flow within the conical gap between the cone and the surface of a rotating disk. *Scientific Reports*, **11**(1), 1–19 (2021)

[25] TURKYILMAZOGLU, M. On the fluid flow and heat transfer between a cone and a disk both stationary or rotating. *Mathematics and Computers in Simulation*, **177**, 329–340 (2020)

[26] TURKYILMAZOGLU, M. The flow and heat in the conical region of a rotating cone and an expanding disk. *International Journal of Numerical Methods for Heat and Fluid Flow*, **3**(6), 2181–2197 (2023)

[27] SRILATHA, P., REMIDI, S., NAGAPAVANI, M., SINGH, H., and PRASANNAKUMARA, B. C. Heat and mass transfer analysis of a fluid flow across the conical gap of a cone-disk apparatus under the thermophoretic particles motion. *Energies*, **16**(2), 952 (2023)

[28] MOATIMID, G. M., MOHAMED, M. A. A., and ELAGAMY, K. A Casson nanofluid flow within the conical gap between rotating surfaces of a cone and a horizontal disk. *Scientific Reports*, **12**(1), 11275 (2022)

[29] WANG, F., RANI, S. P., SARADA, K., GOWDA, R. J. P., KHAN, U., ZAHRAN, H. Y., and MAHMOUD, E. E. The effects of nanoparticle aggregation and radiation on the flow of nanofluid between the gap of a disk and cone. *Case Studies in Thermal Engineering*, **33**, 101930 (2022)

[30] BASAVARAJAPPA, M. and BHATTA, D. Study of the flow of Buongiorno nanofluid in a conical gap between a cone and a disk. *Physics of Fluid*, **34**(11), 112004 (2022)

[31] BASAVARAJAPPA, M. and BHATTA, D. Lie group analysis of flow and heat transfer of nanofluid in cone-disk systems with hall current and radiative heat flux. *Mathematical Methods in the Applied Sciences*, **46**(14), 15838–15867 (2023)

[32] SHEVCHUK, I. V. Laminar heat transfer of a swirled flow in a conical diffuser, self-similar solution. *Fluid Dynamics*, **39**(1), 42–46 (2004)

[33] SHEVCHUK, I. V. Heat and mass transfer in rotating cone-and-disk systems for laminar lows. *Modelling of Convective Heat and Mass Transfer in Rotating Flows*, 127–143 (2016)

[34] SHEVCHUK, I. V. Concerning the effect of radial thermal conductivity in a self-similar solution for rotating cone-disk systems. *International Journal of Numerical Methods for Heat and Fluid Flow*, **33**(1), 204–225 (2022)

[35] RASHIDI, M. M., KAVYANI, N., and ABELMAN, S. Investigation of entropy generation in MHD and slip flow over a rotating porous disk with variable properties. *International Journal of Heat and Mass Transfer*, **70**, 892–917 (2014)

[36] RAJPUT, S., BHATTACHARYYA, K., PANDEY, A. K., and CHAMKHA, A. J. Unsteady axisymmetric flow of nanofluid on nonlinearly expanding surface with variable fluid properties. *JCIS Open*, **8**, 100064 (2022)

[37] JOHN, A. S., MAHANTHESH, B., and SHEVCHUK, I. V. Study of nanofluid flow and heat transfer in a stationary cone-disk system. *Thermal Science and Engineering Progress*, **46**, 102173 (2023)

[38] PAK, B. C. and CHO, Y. I. Hydrodynamic and heat transfer study of dispersed fluids with submicron metallic oxide particles. *Experimental Heat Transfer*, **11**(2), 151–170 (1998)

[39] DAS, S. K., CHOI, S. U., YU, W., and PRADEEP, T. *Nanofluids*: *Science and Technology*, John Wiley & Sons, Chantilly (2007)

[40] ESFE, M. H., ARANI, A. A. A., REZAIE, M., YAN, W. M., and KARIMIPOUR, A. Experimental determination of thermal conductivity and dynamic viscosity of Ag-MgO water hybrid nanofluid. *International Communication in Heat and Mass Transfer*, **66**, 189–195 (2015)

[41] BEECE, D., EISENSTEIN, L., FRAUENFELDER, H., GOOD, D., MARDEN, M. C., REINISCH, L., REYNOLDS, A. H., SORENSEN, L. B., and YUE, K. T. Solvent viscosity and protein dynamics. *Biochemistry*, **19**(23), 5147–5157 (1980)

[42] SHAMPINE, L. F., GLADWELL, I., and THOMPSON, S. *Solving ODEs with MATLAB*, Cambridge University Press, Cambridge (2003)

[43] ANIMASAUN, I. L. Effects of thermophoresis, variable viscosity and thermal conductivity on free convective heat and mass transfer of non-Darcian MHD dissipative Casson fluid flow with suction and nth order of chemical reaction. *Journal of the Nigerian Mathematical Society*, **34**(1), 11–31 (2015)

[44] ZIABAKHSH, Z. and DOMAIRRY, G. Analytic solution of natural convection flow of a non-Newtonian fluid between two vertical flat plates using homotopy analysis method. *Communications in Nonlinear Science and Numerical Simulation*, **14**(5), 1868–1880 (2009)

[45] HATAMI, M. and GANJI, D. D. Natural convection of sodium alginate (SA) non-Newtonian nanofluid flow between two vertical flat plates by analytical and numerical methods. *Case Studies in Thermal Engineering*, **2**, 14–22 (2014)

[46] RAM, P., JOSHI, V. K., SHARMA, K., WALIA, M., and YADAV, N. Variable viscosity effects on time-dependent magnetic nanofluid flow past a stretchable rotating plate. *Open Physics*, **14**(1), 651–658 (2016)

[47] GBADEYAN, J. A., TITILOYE, E. O., and ADEOSUN, A. T. Effect of variable thermal conductivity and viscosity on Casson nanofluid flow with convective heating and velocity slip. *Heliyon*, **6**(1), e03076 (2020)